English
Research Express@NCKU Volume 4 Issue 3 - May 2, 2008
[http://research.ncku.edu.tw/re/articles/e/20080502/6.html]

Low-Frequency Excitation Spectra in Double-Walled Armchair Carbon Nanotubes

M. F. Lin* and Y. H. Ho

Department of Physics, National Cheng Kung University
Email:mflin@mail.ncku.edu.tw

Phys. Rev. B 76, 115422 (2007)

Carbon nanotubes are highly potential materials for nanoscaled electronic devices in the next generation, owing to the peculiar electronic and mechanical properties. Single-walled (m,n) carbon nanotubes are gapless metals or semiconductors depending on radii and chiral angles. Double-walled carbon nanotubes (DWCNTs) are the simplest forms of multiwalled ones. Excitation properties of armchair DWCNTs are investigated in this work. In particular, the intertube atomic hoppings and Coulomb interactions are taken into account simultaneously. The low-energy electronic structure and the distribution of free carriers near the Fermi level are dominated by the symmetric configurations. Their main features would be directly reflected in the single-particle and collective excitations.

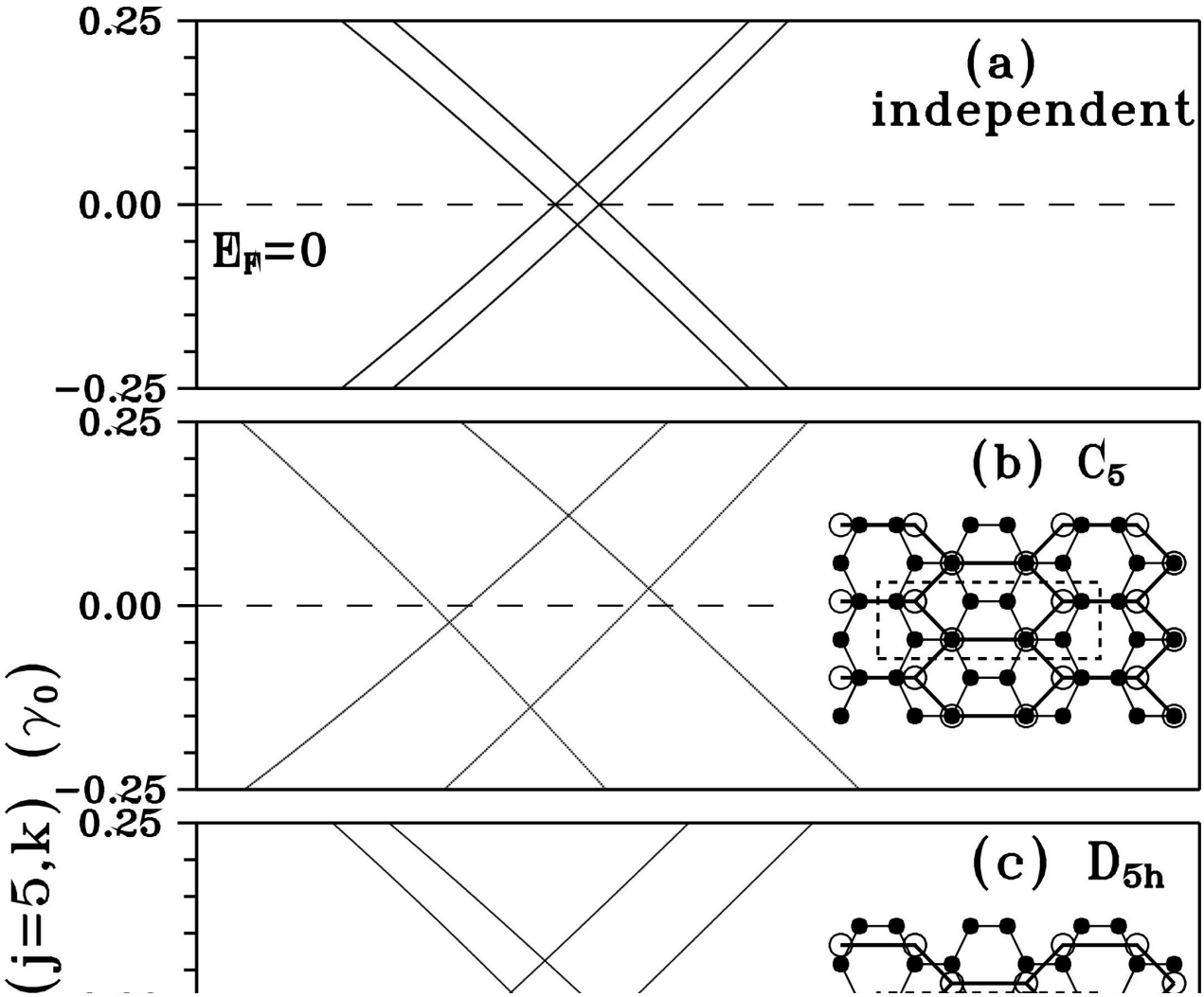

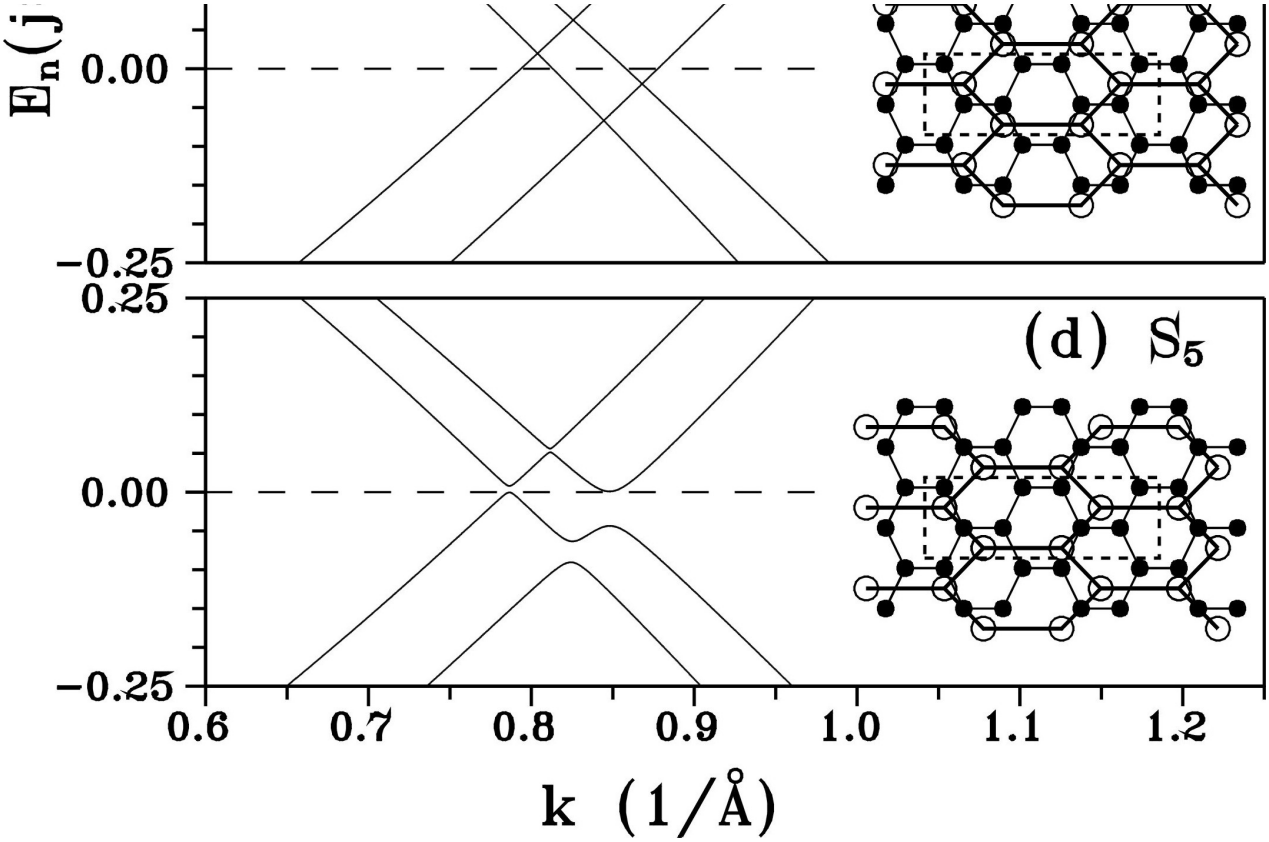

Figure 1. The low energy bands of the double-walled (5,5)-(10,10) carbon nanotubes for three symmetric configurations: (b) C_5, (c) D_{5h}; (d) S_5. Also shown in (a) for comparison are those without the intertube atomic hoppings.

The commensurate armchair DWCNT, (5,5)-(10,10), has three kinds of symmetric structures (C_5,D_{5h} , and S_5 in Figs. 1(b)-(d)). A primitive unit cell consists of four and eight atoms from the inner and outer nanotubes respectively. The π -electronic structure originates from the $2p_z$ orbitals normal to the nanotube surface. The tight-binding Hamiltonian is given by

$$H = \gamma_0 \sum_{l=1}^{2} \sum_{i,i'} h(\theta_{i,l;i',l}) c^{+}_{i,l} c_{i,l} - W \sum_{l \neq l'=1}^{2} \sum_{i,i'} h(\theta_{i,l;i',l'}) e^{-d_{i,l;i',l'}/\delta} c^{+}_{i',l'} c_{i,l} \circ \qquad (1)$$

where $c_{i,l}$ ($c^{+}_{i,l}$) is the creation (annihilation) operator for the *i*th atom on the *l*th nanotube. The first and second terms in Eq. (1), respectively, correspond to the intratube and intertube atomic hoppings. They include the π bonding ($V_{pp\pi}$ =-2.66 eV=r_0) and the σ bonding ($V_{pp\sigma}$ =6.38 eV). The curvature effect due to the misorientation of the $2p_z$ orbitals make the atomic hopping integral $h(\theta_{i,l;i',l'})$ depend on the relative angle $\theta_{i,l;i',l'}$ between two orbitals. The increase of the interatom distance $d_{i,l;i',l'}$ leads to the rapid decrease of the intertube atomic hoppings in the exponential form. Parameters w=1/8 and δ =0.45 Å are obtained from the comparison with the first-principle calculations and the experimental data. By diagonalizing the 12×12 Hamiltonian, we obtain state energy $E_n(j,k)$ and wave function $\varphi_n(j,k) = \sum_{il} u_{n,il}(j,k) a_{i,l}$, with the subband index *n*, the quantized angular momentum *j*, and the longitudinal wave vector *k*. The Bloch function is the superposition of twelve tight-binding functions $a_{l,j}$'s.

The π -electronic structure, without the intertube atomic hoppings, exhibits two pairs of linear subbands intersecting, as shown in Fig. 1(a). The occupied valence bands are symmetric to the unoccupied conduction bands about the Fermi level. Figs. 1(b)-(d) show the effects of the intertube atomic hoppings and the

symmetric configurations on band structures. The symmetry between valence and conduction bands is absent. Energy dispersion relations are linear in C_5 and D_{5h} systems, and change to be parabolic ones in S_5 system with several band-edge states. Both C_5 and D_{5h} systems are gapless metals, while the S_5 system is a narrow-gap semiconductor with E_g~3.2 meV. Apparently, the intertube atomic hoppings in three systems have altered the excitation energies and the carrier distribution. They also induce the strong hybridization of tight-binding functions on the inner and outer nanotubes for electronic states near the Fermi momenta. The carrier tunneling between two different nanotubes is deduced to play an important role in the excitation spectra.

When the DWCNTs are perturbed by the time-dependent Coulomb potential $V^{ex}_{mm'}(q,L)$, their π electrons would screen the external field by the dynamic *e-e* interactions with the momentum *q* and the angular momentum *L* transferred. The effective Coulomb potential between two electrons on the *m*th and *m'*th nanotubes within the RPA, as shown in Fig. 2, is characterized by the Dyson equation

$$\varepsilon_0 V^{eff}_{mm'}(q,L;\omega) = V^{ex}_{mm'}(q,L) + V^{in}_{mm'}(q,L;\omega) = V^{ex}_{mm'}(q,L) + \sum_{m,m'=1}^{2} V^{ex}_{ml}(q,L) P^{(1)}_{ll'}(q,L;\omega) V^{eff}_{l'm'}(q,L;\omega) \circ \quad (2)$$

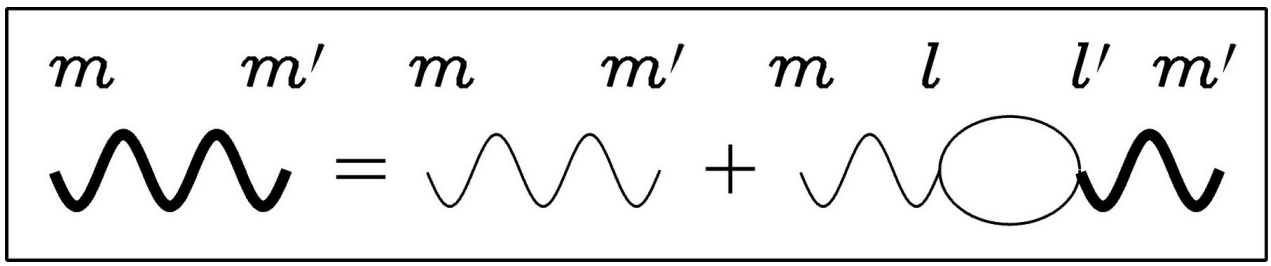

Figure 2. The Feynman diagram of the effective Coulomb potential within the RPA.

ε_0 =2.4 is the background dielectric constant. The effective Coulomb potential is the sum of the external and induced Coulomb potentials. The screening charge density, which causes $V^{in}_{mm'}(q,L;\omega)$, is the product of the bare response function and the effective Coulomb potential. $P^{(1)}_{ll'}(q,L;\omega)$, the RPA bubble in Fig. 2, is given by

$$P^{(1)}_{ll'}(q,L;\omega) = 2\sum_k \sum_{n,n'} \left[\sum_i u_{nli}(j,k) u^*_{nli}(j+L,k+q) \right] \left[\sum_{i'} u^*_{n'li'}(j,k) u_{n'li'}(j+L,k+q) \right] \frac{f[E_n(j,k)] - f[E_{n'}(j+L,k+q)]}{\omega_{nn'}(j,k;j+L,k+q) + \hbar\omega + i\Gamma} \circ$$

(3)

$f(E_n(j,k))$ is the Fermi-Dirac distribution function. $\omega_{nn'}(j,k;j+L,k+q) = E_{n'}(j+L,k+q) - E_n(j,k)$ is excitation energy between the initial and final states. The intratube polarizations ($P^{(1)}_{11}$ and $P^{(1)}_{22}$) and intertube polarizations ($P^{(1)}_{12} = P^{(1)}_{21}$) correspond to the excited electrons and holes on the same and different nanotubes, respectively. The strong hybridization of the inner and outer tight-binding functions makes the intertube polarizations behave as the intratube ones, but with the weaker strength.

The inelastic scattering probability, which is obtained from the detailed calculations within the Born approximation, is used to define the dimensionless loss function

$$\mathrm{Im}\left[\frac{-1}{\varepsilon}\right] = \frac{\sum_m \mathrm{Im}\left[-V^{eff}_{mm}(q,L;\omega)\right]}{\sum_{mm'} V^{ex}_{mm'}(q,L)/2} \circ \quad (4)$$

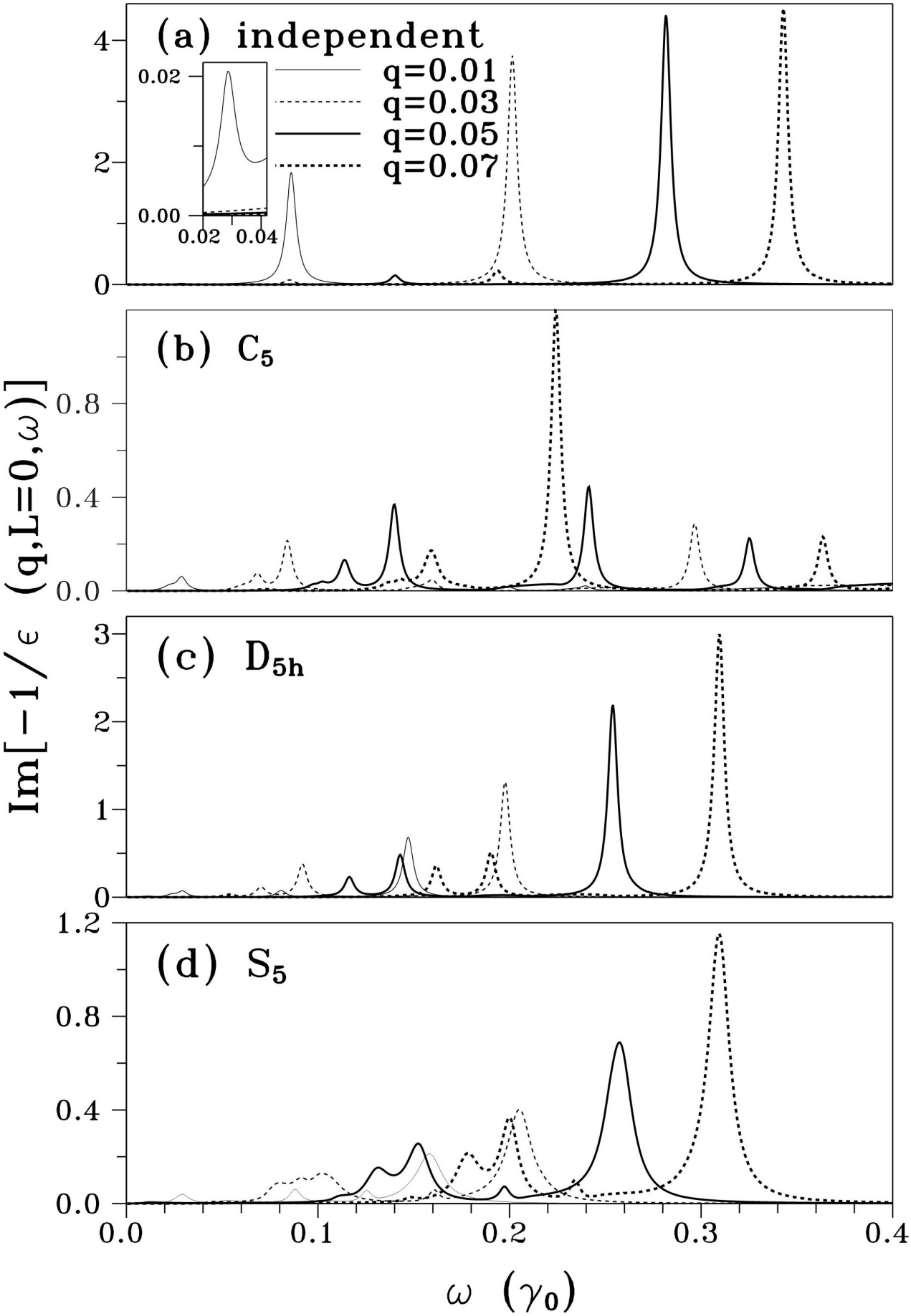

Figure 3. The loss functions at various q's and L=0 for the four systems: (a) independent, (b) C_5, (c) D_{5h}, and (d) S_5.

The denominator is the average value of the external Coulomb potentials on two nanotubes. The screened response function is useful in understanding the low-frequency collective excitations and the measured spectra from Electron Energy Loss Spectroscopy (EELS). The loss spectra of the independent system are shown in Fig. 3(a) for various *q*'s. There are two prominent peaks, and each peak is identified as the collective excitations of charge carriers on two nanotubes. The intertube atomic hoppings bring about more complicated collective excitations, as shown in Figs. 3(b)-3(d). That the π electrons could be excited between any two energy bands is the main reason. The loss spectra exhibit more plasmon peaks, while their intensities are reduced by the rich single-particle excitations. Each plasmon mode is associated with a specific excitation channel from the critical point. Some plasmon modes might disappear in the increasing of *q* because of the strong Landau damping. However, a simple relation between the frequency and the strength is absent in three kinds of symmetric configurations.

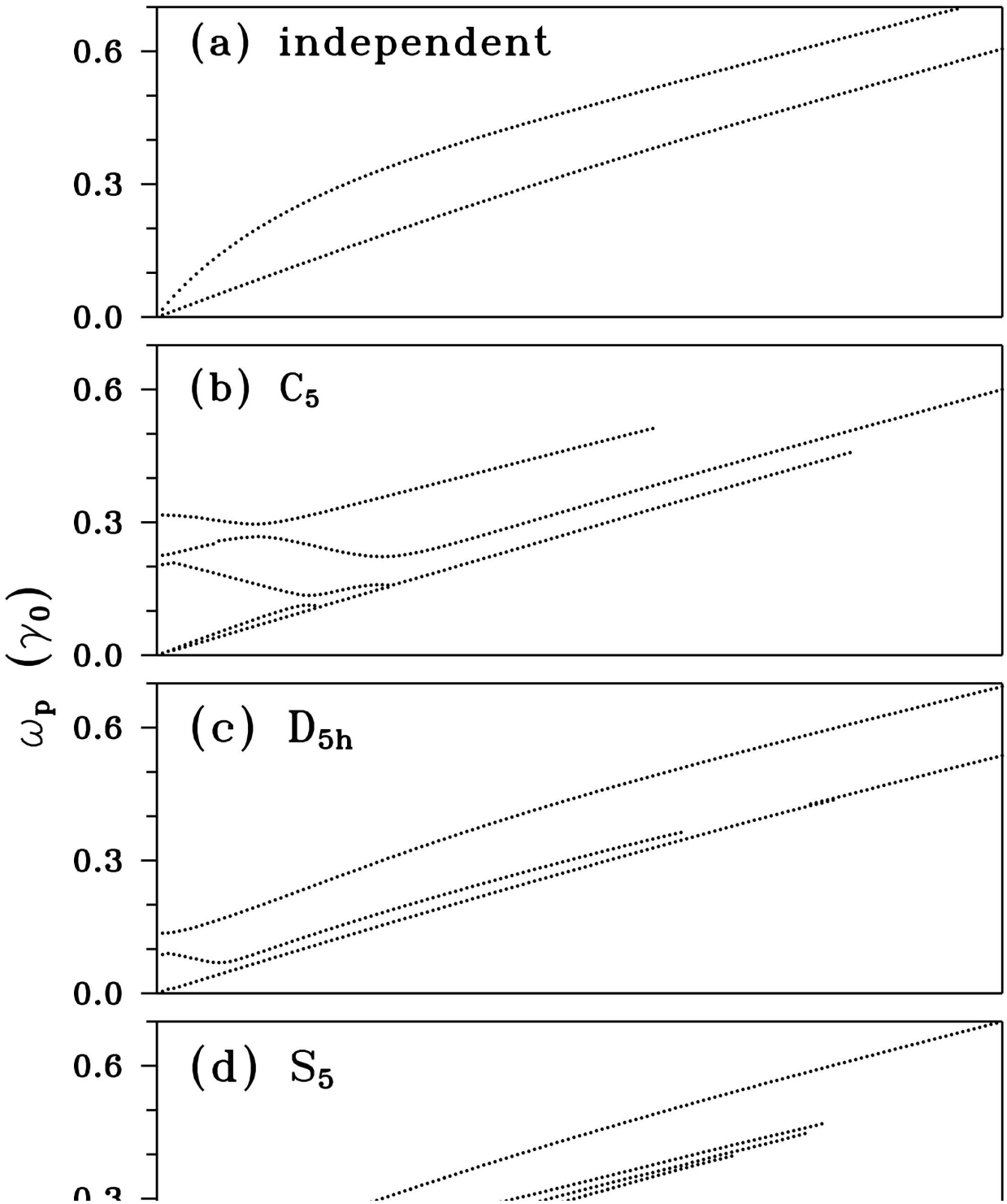

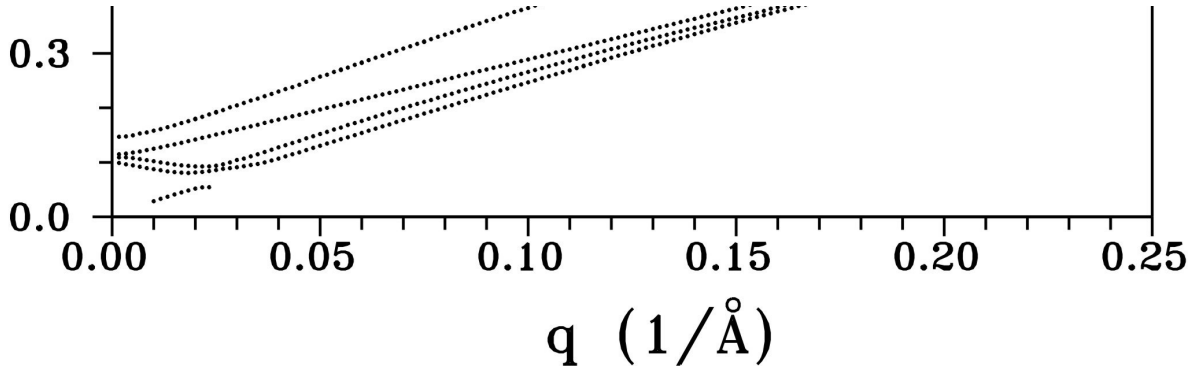

Figure 4. The momentum-dependent plasmon frequencies for the (a) independent, (b) C_5, (c) D_{5h}, and (d) S_5systems.

The transferred momentum dominates the main features of the low-frequency plasmons. Plasmons are quanta of collective electron density oscillations. They belong to acoustic (optical) modes, when their frequencies are vanishing (finite values) at long wavelength limit $q \to 0$. There exist only two acoustic plasmons in the independent systems, and they could survive at large q's (Fig. 4(a)). The intertube atomic hoppings drastically change the acoustic plasmons and create several optical plasmons, as shown in Figs. 3 (b)-3(d). The former are completely suppressed by the serious *e*-*h* damping for q higher than the critical momentum. The absence of acoustic plasmon in the S_5 system lies in the narrow-gap characteristic. Most of plasmons in three symmetric systems belong to optical modes, since the single-particle excitation energies related to the critical points have finite values.

In summary, the low-frequency excitations are studied for armchair DWCNTs. The intertube atomic hoppings and Coulomb interactions are included in the calculations. The former significantly affect the low energy bands and thus enrich the excitation spectra. The wave-vector dependence, critical points, and energy gap of energy bands dominate the main characteristics of the bare and screened response functions. The intertube atomic hoppings induce more single-particle excitation channels and plasmon modes, mainly owing to the Fermi-momentum states or the band-edge states. The plasmon strength is reduced by the intertube carrier tunneling. The number, frequency, strength, and momentum dependence of plasmon modes strongly rely on the symmetric configurations. Most of plasmons belong to optical modes, but not acoustic modes. The experimental measurements of EELS are predicted to be useful in determining the double-walled geometric structures.

Copyright 2009 National Cheng Kung University